Article

Cell Reports

Impaired Spermatogenesis, Muscle, and Erythrocyte Function in U12 Intron Splicing-Defective *Zrsr1* Mutant Mice

Graphical Abstract

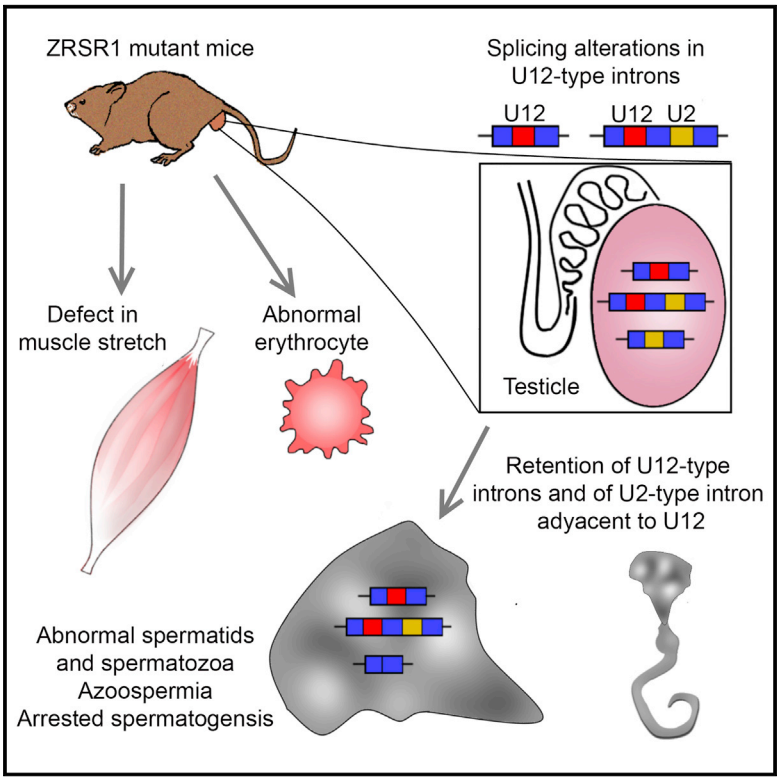

Highlights

- ZRSR1^{mu} produces severe defects in erythrocytes, muscle stretch, and spermatogenesis
- Spermatogenesis defects of ZRSR1^{mu} are due to splicing alteration in U12-type intron
- ZRSR1^{mu} causes retention of most of the U12-type introns examined
- ZRSR1 is implicated also in removal of U2 introns positioned adjacent to a U12 intron

Authors

Keiko Horiuchi, Serafín Perez-Cerezales, Panagiotis Papasaikas, ..., Belén Pintado, Juan Valcárcel, Alfonso Gutiérrez-Adán

Correspondence

juan.valcarcel@crg.eu (J.V.), agutierr@inia.es (A.G.-A.)

In Brief

Horiuchi et al. report that mutations in *Zrsr1* cause defects in blood, muscle, and spermatogenesis. The molecular basis for the spermatogenesis defect is the *Zrsr1* involvement in processing U12-type introns (minor splicing), causing retention of most of the U12 introns examined.

Data and Software Availability

E-MTAB-4872

Horiuchi et al., 2018, Cell Reports *23*, 143–155
April 3, 2018
https://doi.org/10.1016/j.celrep.2018.03.028

CellPress

Cell Reports
Article

Impaired Spermatogenesis, Muscle, and Erythrocyte Function in U12 Intron Splicing-Defective *Zrsr1* Mutant Mice

Keiko Horiuchi,[1,2,3,11] Serafín Perez-Cerezales,[4,11] Panagiotis Papasaikas,[1,2] Priscila Ramos-Ibeas,[4] Angela Patricia López-Cardona,[4] Ricardo Laguna-Barraza,[4] Noelia Fonseca Balvís,[4] Eva Pericuesta,[4] Raul Fernández-González,[4] Benjamín Planells,[4] Alberto Viera,[5] Jose Angel Suja,[5] Pablo Juan Ross,[6] Francisco Alén,[7] Laura Orio,[7] Fernando Rodriguez de Fonseca,[7,8] Belén Pintado,[9] Juan Valcárcel,[1,2,10,12,*] and Alfonso Gutiérrez-Adán[4,12,13,*]

[1]Centre for Genomic Regulation (CRG), The Barcelona Institute of Science and Technology, Dr. Aiguader 88, 08003 Barcelona, Spain
[2]Universitat Pompeu Fabra, Dr. Aiguader 88, 08003 Barcelona, Spain
[3]Department of Quantitative Biology and Medicine, Research Center for Advanced Science and Technology (RCAST), University of Tokyo, Tokyo 153-8904, Japan
[4]Dpto. de Reproducción Animal, INIA, Avda Puerta de Hierro no 12. Local 10, 28040 Madrid, Spain
[5]Unidad de Biología Celular, Departamento de Biología, Facultad de Ciencias, Universidad Autónoma de Madrid, Madrid, Spain
[6]Department of Animal Science, University of California, Davis, Davis, CA, USA
[7]Dpto. Psicobiología, Facultad de Psicología, UCM, Campus de Somosaguas, Madrid, Spain
[8]UGC Salud Mental, Instituto de Investigación Biomédica de Málaga (IBIMA), Universidad de Málaga-Hospital Universitario Regional de Málaga, Avda. Carlos Haya 82, Pabellón de Gobierno, 29010 Málaga, Spain
[9]Servicio de Transgénicos, CNB-CSIC, UAM, Madrid, Spain
[10]Institució Catalana de Recerca i Estudis Avançats (ICREA), Pg. Lluís Companys 23, 08010 Barcelona, Spain
[11]These authors contributed equally
[12]Senior author
[13]Lead Contact
*Correspondence: juan.valcarcel@crg.eu (J.V.), agutierr@inia.es (A.G.-A.)
https://doi.org/10.1016/j.celrep.2018.03.028

SUMMARY

The U2AF35-like ZRSR1 has been implicated in the recognition of 3′ splice site during spliceosome assembly, but ZRSR1 knockout mice do not show abnormal phenotypes. To analyze ZRSR1 function and its precise role in RNA splicing, we generated ZRSR1 mutant mice containing truncating mutations within its RNA-recognition motif. Homozygous mutant mice exhibited severe defects in erythrocytes, muscle stretch, and spermatogenesis, along with germ cell sloughing and apoptosis, ultimately leading to azoospermia and male sterility. Testis RNA sequencing (RNA-seq) analyses revealed increased intron retention of both U2- and U12-type introns, including U12-type intron events in genes with key functions in spermatogenesis and spermatid development. Affected U2 introns were commonly found flanking U12 introns, suggesting functional cross-talk between the two spliceosomes. The splicing and tissue defects observed in mutant mice attributed to ZRSR1 loss of function suggest a physiological role for this factor in U12 intron splicing.

INTRODUCTION

Alternative splicing (AS) of messenger RNA precursors (pre-mRNAs) is one of the mechanisms whereby a single gene produces distinct mRNAs, contributing to proteome diversity in complex organisms (Nilsen and Graveley, 2010). Alterations in AS are often associated with disease (Daguenet et al., 2015; Scotti and Swanson, 2016). Ninety-five percent of multi-exon mammalian genes undergo AS (Pan et al., 2008; Wang et al., 2008). The splicing machinery comprises five small, nuclear ribonucleoprotein particles (snRNPs). The major splicing machinery (termed U2 spliceosome, composed of U1, U2, and U5/4/6 snRNPs) removes the majority of introns, while the minor (or U12) spliceosome (composed of U11, U12, U5/4atac/6atac snRNPs) removes <0.5% of all introns (Burge et al., 1998). U12-type introns coexist with U2-type introns in essential genes (Patel and Steitz, 2003). Splicing factors ZRSR1/2 have been implicated in 3′ splice site recognition of both U2 and U12 introns (Shen et al., 2010). Recent sequencing studies have revealed frequent somatic ZRSR2 mutations in hematological malignancies such as myelodysplastic syndrome (MDS) (Madan et al., 2015). However, the physiological role of ZRSR1 remains unclear.

Zrsr1 is an intronless gene located in mouse chromosome 11 and human chromosome 5. Murine *Zrsr1* is a retrotransposed copy of X-linked *Zrsr2*. *Zrsr1* is located within an intron of *Commd1* (Figure 1A) and is paternally expressed in the placenta

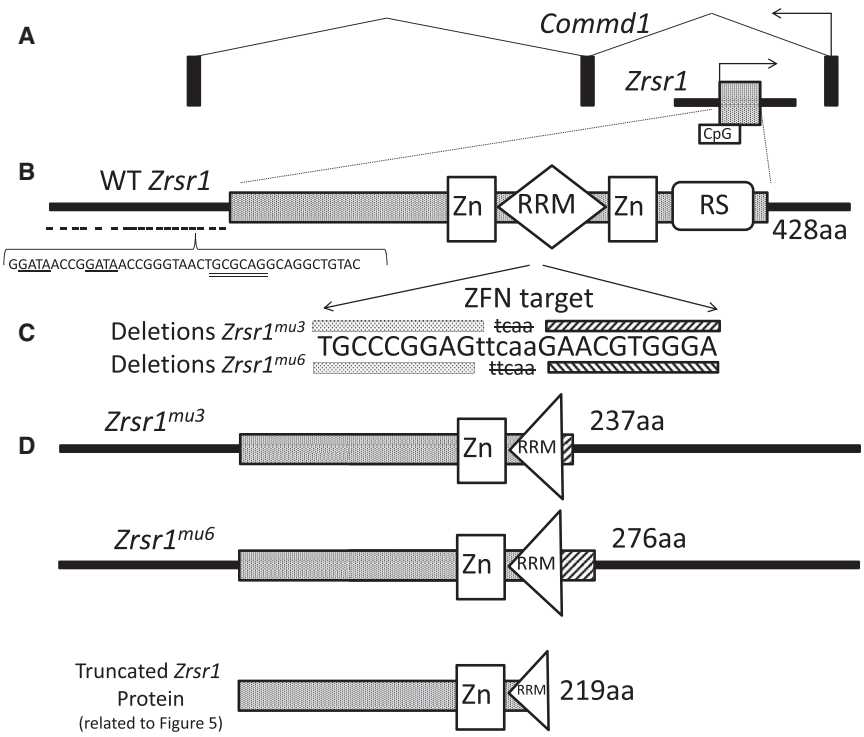

Figure 1. Diagrams of *Zrsr1* Gene Structure and Mutations Produced by Zinc Finger-Mediated Mutagenesis in Transgenic Mice

(A) The *Commd1* gene consists of three exons (vertical bars) and the imprinted gene, *Zrsr1*, located in the first intron; a CpG island is shown as a solid box. Arrows indicate the transcriptional direction of the genes.

(B) Diagram of the *Zrsr1* gene with its functional domains: Zn (zinc finger), RRM (RNA recognition motif), and RS (arginine-serine rich). The sequence indicated in the promoter region containing two GATA regions is repeated 19 times in the closest promoter region; the sequence also contains a NRF1 recognizing sequence (double underlined).

(C) Nucleotide deletions produced by zinc finger nucleases in the transgenic mice lines *Zrsr1*^{mu3} and *Zrsr1*^{mu6}. Blocks indicate nucleotides remaining in the mutant, while residues outside the blocks are deleted nucleotides.

(D) Diagrams of the domains present in the mutated *Zrsr1* proteins in the two transgenic mice lines. Transgenic mice expressed a mutated short Zrsr1 protein also containing a Zn domain and part of the RRM domain. The numbers indicate amino acids encoded by the mutant proteins.

and some adult tissues, while the maternal copy is methylated and silent (Nabetani et al., 1997). *Zrsr1* encodes a protein that is highly homologous to the 35 kDa subunit of the evolutionarily conserved heterodimeric splicing factor U2AF. U2AF is composed of U2AF65 and U2AF35, which play critical roles in recognition of the polypyrimidine tract and the 3′ splice site AG, respectively. In mammals, U2AF35 is encoded by the *U2AF1* gene and U2AF35-related proteins include U2AF26 (encoded by the *U2AF1L4* gene), ZRSR1 (also known as U2af1-rs1) and ZRSR2 (also known as U2af1-rs2) (encoded by the *ZRSR1* and *ZRSR2* genes). The 4 proteins are paralogs and contain 2 CCCH zinc finger motifs and one RNA-recognition motif (RRM) located between the two CCCH domains (Figure 1B). U2AF35 family members are expressed in multiple tissues during development. In most tissues, there is redundant expression of more than one protein. It has been observed that *Zrsr1* knockout mice do not show an abnormal phenotype (Sunahara et al., 2000), probably because of the compensatory expression of one or more of the other 3 paralogs.

To examine the role of ZRSR1 *in vivo*, we generated *Zrsr1* mutant mice containing nonsense mutations in the RNA-recognition motif. These mice show the predicted expression of truncated proteins containing one of the zinc finger (CCCH) domains, which could potentially exert a dominant negative effect on ZRSR1 function (Figures 1C and 1D). Homozygous mutants exhibit severe defects in erythrocyte maturation, muscle strength, and spermatogenesis, the latter including germ cell sloughing and apoptosis, ultimately leading to azoospermia and male sterility. RNA sequencing (RNA-seq) of mouse testis on day 15 revealed enhanced intron retention as the most frequent splicing alteration, affecting mainly U12 introns but also U2 introns, typically those positioned adjacent to a U12 intron. Further analyses, including rescue experiments in cell culture, revealed that the mutation gave rise to retention of most of the U12 introns examined. This study identifies a role for ZRSR1 in U12 intron splicing with effects on spermatogenesis, muscle strength, and erythrocyte development.

RESULTS

Zrsr1 mRNA Expression in Development and Adult Tissues

We first analyzed the expression of *Zrsr1* during preimplantation development and in different adult mouse tissues. *Zrsr1* was expressed at the 2-cell stage (at the time of genome activation), and at the morula and blastocyst stages, when male blastocysts showed higher *Zrsr1* expression levels than female blastocysts (Figure 2A). Similar expression profiles were observed in the cow and pig, although the ortholog to *Zrsr1* (*ZRSR2Y*) is only expressed in male embryos (Bermejo-Alvarez et al., 2010) (Figure S1A) suggesting a possible role in early sex-developmental pathways in these species. We detected higher expression of *Zrsr1* in placenta than in embryo on days 8 and 14, without differences between sexes. In adult tissues, highest expression levels were observed in the brain, and lower expression levels in other tissues like epididymis, testis, bone marrow, or muscle (Figure 2B). In developing testis, *Zrsr1* expression was detected in both Sertoli and spermatogenic cells; peak expression was observed on days 9 and 15 when the seminiferous epithelium contains spermatogonia, spermatocytes, and Sertoli cells, and

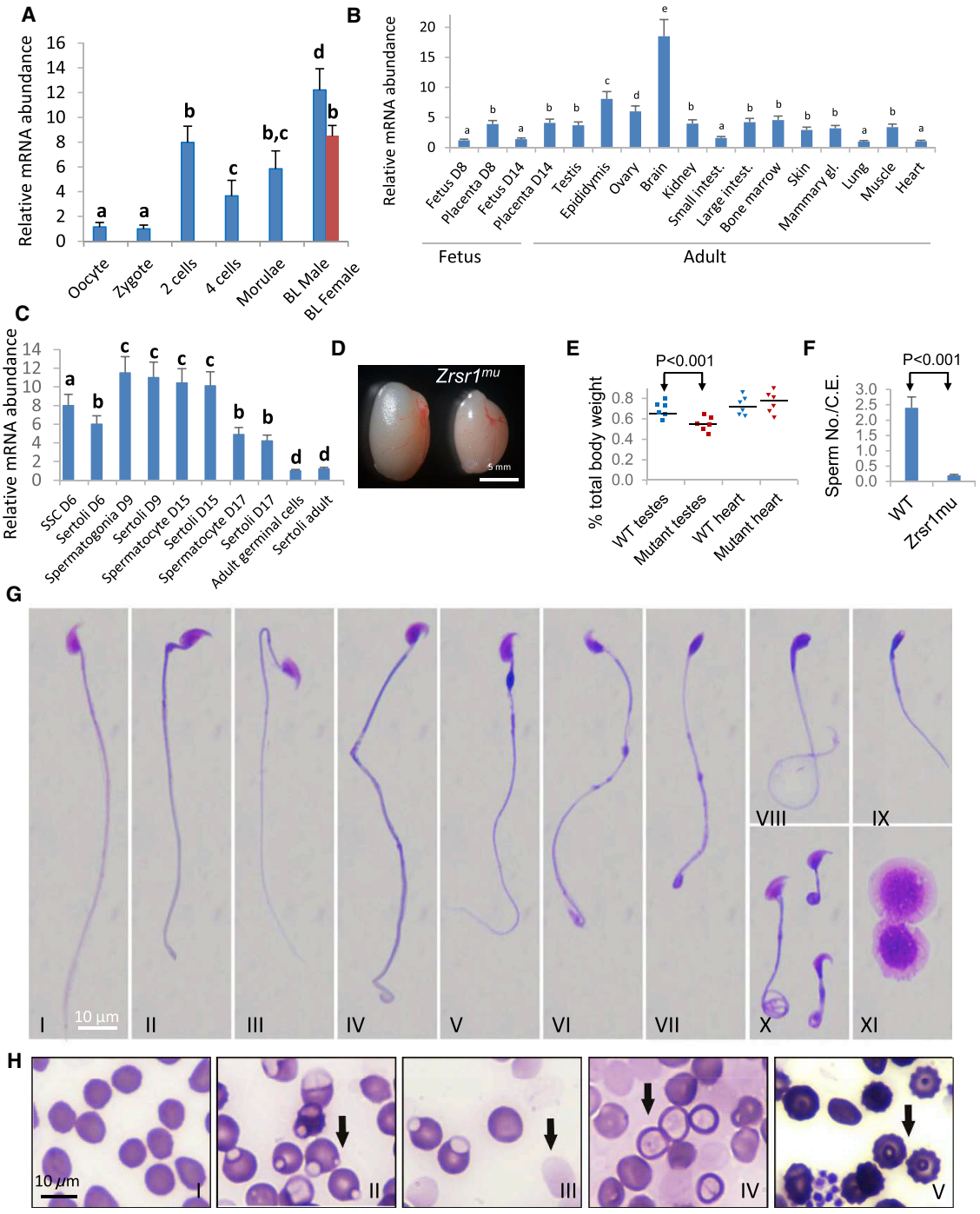

Figure 2. RNA Expression of *Zrsr1* and Phenotypic Abnormalities of Transgenic *Zrsr1* Mutant in Testis, Sperm, and Erythrocytes

(A) Relative expression levels of *Zrsr1* during preimplantation embryo development determined by qPCR. Biological triplicate results are presented as mean ± SEM. Bars with different superscripts differ significantly ($p < 0.05$); BL, blastocysts.

(B) Relative expression levels of *Zrsr1* in fetus and placenta (D8 and D14) and in different adult tissues determined by qPCR. Biological triplicate data for qPCR are presented as mean ± SEM. Bars with different superscripts differ significantly ($p < 0.05$).

(C) Relative expression level of *Zrsr1* during testis development in germinal cells and Sertoli cells determined by qPCR. Biological triplicate data for qPCR are presented as mean ± SEM. Bars with different superscripts differ significantly ($p < 0.05$).

(D) *Zrsr1*^{mu} and WT littermate testis from 12-week-old mice.

(E) WT (blue, n = 6) and mutant *Zrsr1*^{mu} (red, n = 6) testes and heart size shown as a percentage of total body weight in 12-week-old mice.

(F) Comparison of average sperm numbers per cauda epididymis (C.E.) in 12-week-old WT (n = 6) and *Zrsr1*^{mu} mice (n = 6).

(legend continued on next page)

more reduced expression was noted on day 17, when most spermatogenic cells have reached the spermatocyte stage (Bellvé et al., 1977) and in adult testis (Figure 2C).

Zrsr1 Mutant Male Mice Display Severe Defects in Spermatogenesis

It has been reported that *Zrsr1* knockout animals do not display altered phenotypes (Sunahara et al., 2000) possibly because of the compensating effects of one or more of the other 3 paralogs (*U2af1*, *U2af1l4*, *Zrsr2*). For this reason, we used a zinc finger nuclease strategy to generate *Zrsr1* mutant mice containing nonsense mutations in the RNA-recognition motif, thus leading to a predicted protein which could potentially exert a dominant negative effect on ZRSR1 function (Figures 1C and 1D). Two different transgenic mouse lines harboring 4- and 5-nucleotide deletions (*Zrsr1*^{mu3} and *Zrsr1*^{mu6}, respectively) were therefore created to produce truncated proteins containing only one zinc finger domain and part of the RNA-recognition motif (Figures 1C and 1D). Because both lines showed similar phenotypes, the following phenotypic results refer to the *Zrsr1*^{mu3} line, and all the animals analyzed were homozygous for the mutation. Expression of the wild-type and mu3 truncated proteins was detected by targeted proteomics (see below).

Male and female transgenic mice developed normally, but 95% of male mutants carrying the mutation in homozygosity were sterile. The testes of adult mice were smaller than in controls, sperm counts were low (Figures 2D–2F), and sperm showed abnormalities including neck and midpiece defects (Figure 2G, II–VII), head defects (Figure 2G, VII–IX), and tail defects (Figure 2G, IV–X). Histological observation of *Zrsr1*^{mu3} testis revealed some seminiferous tubules arrested at the spermatocyte stage, few spermatids and spermatozoa (Figures 3A–3C and S2) germ cell sloughing, and a high level of apoptosis (Figures 3G and 3H). This ultimately would lead to azoospermia and male sterility. The epididymis and vas deferens only showed spermatocytes, spermatids, and a small amount of spermatozoa (Figures 3D–3F; Video S1). Surprisingly ~5% of the young transgenic mice were fertile until 5–6 months of age and then became sterile, while no correlation was detected between fertility and DNA methylation status at the imprinting oocyte-specific CpG island of the promoter and first part of the *Zrsr1* exon (Figure 1A), previously correlated with *Zrsr1* expression (Hayashizaki et al., 1994). Evaluation of the three *Zrsr1* paralogs in adult testis revealed increased expression of *Zrsr2* in fertile males (Figure S1B), suggesting that abnormal escape of *Zrsr2* from X chromosome inactivation (XCI) could be responsible for the low proportion of *Zrsr1*^{mu3} fertile mice. Interestingly *Zrsr2* has been reported to escape XCI in other tissues in mice (Li et al., 2016; Marks et al., 2015). No difference in mRNA expression was observed in Sertoli cells (Figure S1C). Immunocytochemical analyses of MEI1, a gene required for normal meiotic chromosome synapsis (Sato et al., 2006), in testis of wild-type (WT) and *Zrsr1*^{mu3} mice showed lower percentage of tubules and cells expressing MEI1 in the mutant (Figure S2). Although normal meiosis could be observed in some cells of the *Zrsr1*^{mu3} testicles, most spermatids presented a severely altered nuclear morphology (Figure S3). Normal histology was observed at day 15 in mutant mice (Figure S1D).

Rescuing Spermatogenesis in *Zrsr1* Mutant Mice through Spermatogonia Transplantation

To determine whether germinal cells or Sertoli cells were responsible for the spermatogenic defect observed in *Zrsr1*^{mu3} we performed spermatogonia transplantations to recipient mice in which endogenous spermatogenesis had been inhibited by busulfan treatment (Avarbock et al., 1996). Spermatogonia from prepubertal WT mice (6 days of age) were transferred to the busulfan-treated testes of *Zrsr1*^{mu} adult mice and vice versa. Spermatogonia from transgenic mice with EGFP-tagged X chromosomes (Nakanishi et al., 2002) were transferred into *Zrsr1*^{mu} mice (Figures S4A and S4C) and spermatogonia from double transgenic mice carrying EGFP and *Zrsr1*^{mu} alleles transferred into WT mice (Figures S4B and S4D). As expected, busulfan-treated testes lacked germ cells but contained Sertoli cells lining the seminiferous tubule. However, after donor cell transplantation from either WT or *Zrsr1*^{mu} mice (n = 17 and n = 31, respectively), green fluorescent tubules were found containing germ cell elements (n = 11 and n = 25 showed GFP-positive cells in *Zrsr1*^{mu} and WT recipient mouse testes, respectively) (Figure S4). However, while WT spermatogonia transplanted in *Zrsr1*^{mu} mice were able to produce spermatozoa (Figures S4A, S4C, and S4E–S4H), *Zrsr1*^{mu} spermatogonia colonized seminiferous tubules but did not produce spermatozoa (Figures S4B, S4D, S4I, and S4J). These results indicate that germinal cells are affected in *Zrsr1*^{mu} mice, and mutant Sertoli cells are able to recover the spermatogenesis capacity of WT transplanted spermatogonia.

Zrsr1 Mutant Male Mice Feature Severe Red Blood Cell and Muscle Strength Defects

Among the 4 U2AF35-related splicing factors (*U2af1*, *U2af1l4*, *Zrsr1*, *Zrsr2*), *Zrsr1* was found to show the highest mRNA levels in erythrocytes from WT and *Zrsr1*^{mu} mice (Figure S5A). Hematological evaluation showed that *Zrsr1*^{mu} mice had fewer red blood cells, a lower amount of hemoglobin, and lower hematocrit (Table S2), without differences in erythrocyte volume, hemoglobin content, and erythrocyte hemoglobin. Red blood cell morphology was also affected: 75% of males (n = 20) showed 20%–25% of erythrocytes with different abnormalities (Figure 2H), mostly blister cells, ghost cells, hypochromic cells, and echinocyte cells (Figure 2H). These data indicate a role for *Zrsr1* in erythrocyte production and maturation. In addition, *Zrsr1*^{mu} mice showed increased numbers of lymphocytes, which could be attributed to lymphocyte leukemia, although the animals appeared healthy.

(G) Examples of normal (I) and abnormal (II–XI) sperm isolated from the cauda epididymis in *Zrsr1*^{mu} mice (stained with Diff-Quik and observed under a standard bright-field microscope). Over 80% of sperm display some type of abnormality including neck and midpiece defects (II–VII), head defects (VII–IX), tail defects (IV–X), and immature cells (XI).

(H) Blood smear (methylene blue staining) showing normal erythrocytes (I) in WT mice and some abnormalities in *Zrsr1*^{mu} mice like blister cells (II, arrow indicates a vacuole), ghost cells (III, indicated by arrow), hypochromic cells (IV, indicated by arrow), and echinocytes (V, indicated by arrow).

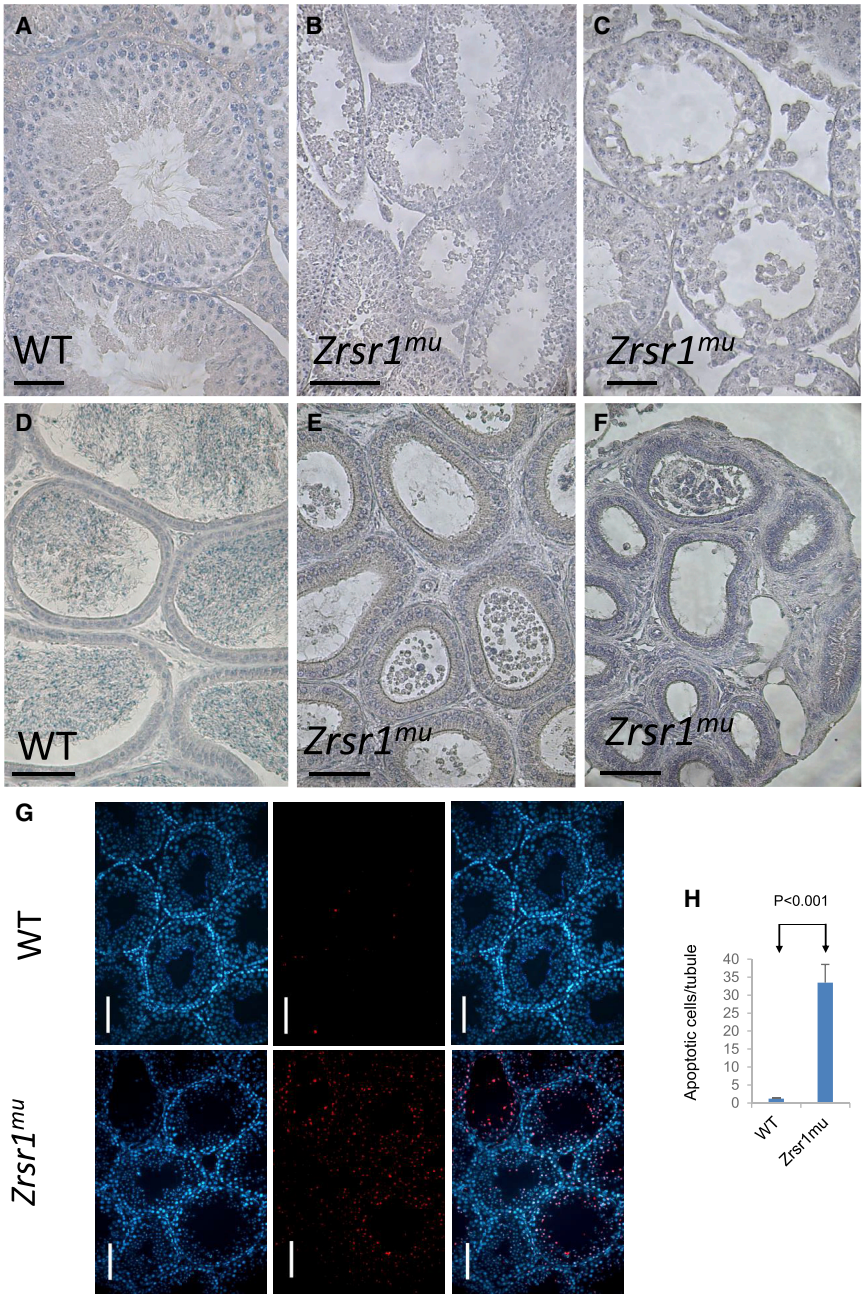

Figure 3. Histology of WT and Transgenic Mice Testis at 3–4 Months of Age from Testis, Epididymis, and Efferent Ducts

(A) HE staining of a WT testis section. Scale bar, 40 μm.

(B) HE staining of a *Zrsr1*^{mu} testis section showing severe disruption of seminiferous tubule architecture. Scale bar, 100 μm.

(C) Magnification of a *Zrsr1*^{mu} testis section. Scale bar, 40 μm.

(D) HE staining of the cauda epididymis in a section from a WT animal. Scale bar, 100 μm.

(E) HE staining of the caput epididymis containing immature germ cells in a *Zrsr1*^{mu} animal. Scale bar, 50 μm.

(F) HE staining of efferent ducts from *Zrsr1*^{mu} that appear empty or containing immature germ cells. Scale bar, 50 μm.

(G) Hoechst, TUNEL staining, and merge of testis sections from WT and *Zrsr1*^{mu} showing apoptotic cells in the seminiferous tubules. Scale bar, 100 μm.

(H) Mean ± SEM (n = 6) apoptotic cells in each seminiferous tubule of WT and *Zrsr1*^{mu} mice.

mRNA expression analysis of the 4 splicing factors (*U2af1*, *U2af1l4*, *Zrsr1*, *Zrsr2*) in the quadriceps femoris of WT and *Zrsr1*^{mu} mice revealed the higher expression of *U2af1* compared to the remaining paralogs (Figure S5B) and also the higher expression of this gene in mutant mice compared with WT mice (Figure S5B). Motor performance/coordination (balance beam) tests in *Zrsr1*^{mu} revealed no differences with WT mice at both 4 and 10 months of age. However, *Zrsr1*^{mu} mice showed significant deficits in grip strength in wire-hang tests relative to WT animals at 4, but especially, at 10 months of age (Figure S5C), suggesting age-related loss of muscle function. Mutant mice showed an increase in the number of fibers of larger cross-sectional area, an increase in average fiber area in the quadriceps femoris (Figure S5E) and a reduction in the total number of fibers (Figure S5E). No other histological alterations were observed in either muscle structure or collagen amount (Figure S5D).

To explore whether the reduced muscle strength could be related to skeletal muscle calcium content, we determined total intracellular Ca^{2+} for the extensor *digitorum longus* (EDL) and tibialis anterior using Ca-dependent UV absorbance spectra of the Ca^{2+} chelator 1,2-bis(2-aminophenoxy)ethane-N,N,N′,N′-tetraacetic acid (BAPTA) (Lamboley et al., 2015). We found higher EDL muscle Ca^{2+} contents in *Zrsr1*^{mu} mice (Figure S5F). In Fluo-4 calcium assays, Ca^{2+} releases from sarcoplasmic reticulum (SR) after transient hypo-osmotic stress were significantly reduced in *Zrsr1*^{mu} mice (Park et al., 2014) (Figure S5G) suggesting that these abnormalities in Ca^{2+} flux across the sarcolemma could be the reason for the reduced muscular strength shown by the mutant mice.

ZRSR1^{mu3} Protein Cannot Compensate for the Loss of ZRSR Function

To directly assess the function of the truncated ZRSR1^{mu3} protein, reconstitution experiments were conducted. Endogenous ZRSR1 and ZRSR2 proteins were small interfering RNA (siRNA)-knocked down in HEK293 cells and tetracycline used to induce the expression of N-terminally V5-tagged human

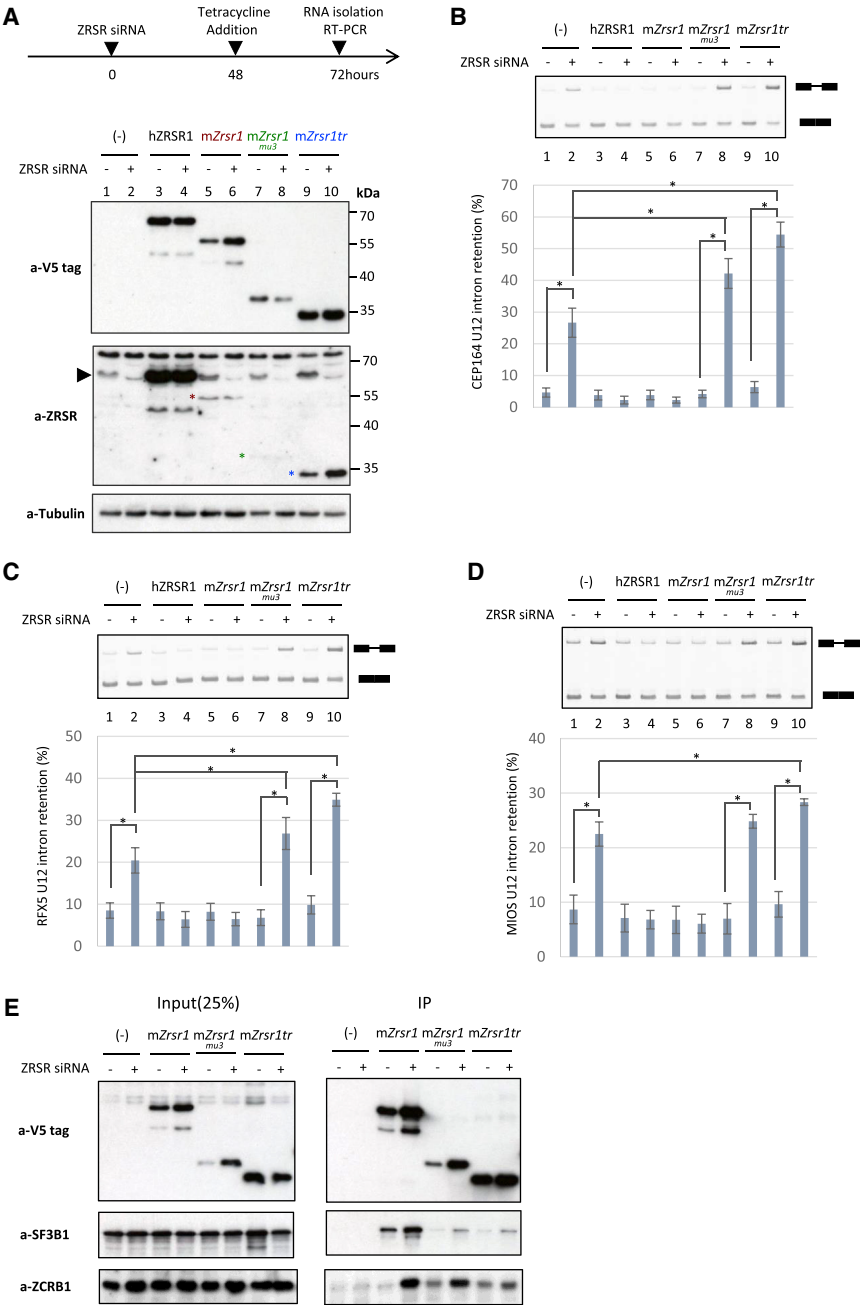

Figure 4. Reconstitution System Reveals that ZRSR1^{mu3} Is Defective in U12 Intron Splicing

(A) Experimental design and protein expression. Timeline of ZRSR proteins knock down, tetracycline-inducible expression of ZRSR1, and protein variants and RNA isolation. Lower panels: western blot analysis of ZRSR protein expression (arrowhead indicates endogenous ZRSR1 and ZRSR2, and siRNA-resistant human ZRSR1 [lanes 3 and 4], colored asterisks indicate mZrsr1, ZRSR1^{mu3} and mZrsr1truncated protein, which display limited reactivity with anti-human ZRSR2 antibody), recombinant V5-tagged expression and tubulin as loading control. The positions of molecular mass markers are indicated on the right.

(B) RT-PCR analysis of CEP164 U12 intron 32 retention. RNA samples from the reconstitution assays shown in (A) were analyzed using primers complementary to the exons flanking the intron. The position of intron retention and spliced PCR products after acrylamide gel electrophoresis are indicated. Lower panel shows the quantification of the percentage of intron retention for six biological replicates.

(C and D) Equivalent analyses to (B), for U12 intron 7 of RFX5 (C) and intron 4 of MIOS (D) genes. The values are the average ± SD (error bars), n = 6, *p < 001 by two-way ANOVA followed by Tukey's post hoc test.

(E) Immunoprecipitation-western blotting (IP-WB) analysis to detect interaction of V5-tagged ZRSR1 with SF3B1 and ZCRB1. Whole cell lysates from the reconstitution assays shown in (A) were used for IP.

ZRSR1, mouse ZRSR1, ZRSR1^{mu3}, or a truncated ZRSR1 protein corresponding to the N-terminal 219 amino acids. Each protein was expressed from the same single genomic locus in stable cells lines constructed by targeted flip-in genome editing. In these cell lines, the exogenous proteins were mostly expressed at levels 3- to 4-fold higher than endogenous ZRSR1 and ZRSR2 proteins, although ZRSR1^{mu3} accumulated at comparatively lower levels (Figure 4A), suggesting lower protein accumulation/stability of ZRSR1^{mu3} compared to the WT protein, likely contributing to the mutant phenotypes. RNA was isolated 24 hr after tetracycline induction, and the splicing of several U12 introns was examined by RT-PCR. Consistent with prior reports of mis-splicing of U12 introns in patients with myelodysplastic syndrome (MDS) (Madan et al., 2015) with ZRSR2 mutations, the depletion of ZRSR proteins led to enhanced retention of the *Cep164* U12 intron (Figure 4B, compare lanes 1 and 2). Similar results were obtained for other U12 introns of the *Rfx5* or *Mios* genes (Figures 4C and 4D and see below). These effects were rescued upon expression of human or mouse ZRSR1 proteins (compare lanes 2 with 4 and 6 in Figures 4B–4D), but not by the expression of ZRSR1^{mu3} nor of the slightly shorter truncated ZRSR1 (lanes 8 and 10 in Figures 4B–4D). Collectively, these results suggest that ZRSR1^{mu3} protein is defective at promoting U12 intron splicing. Interestingly, the expression of ZRSR1^{mu3} or the truncated (219 amino acids) ZRSR1 exacerbated the effect of ZRSR-protein knock down in the *Cep164* intron (Figure 4B, compare lanes 2 with 8 or 10), suggesting the mutant exerts a dominant-negative effect in some substrates.

To start analyzing the molecular mechanisms behind these observations, we carried out immunoprecipitation and western

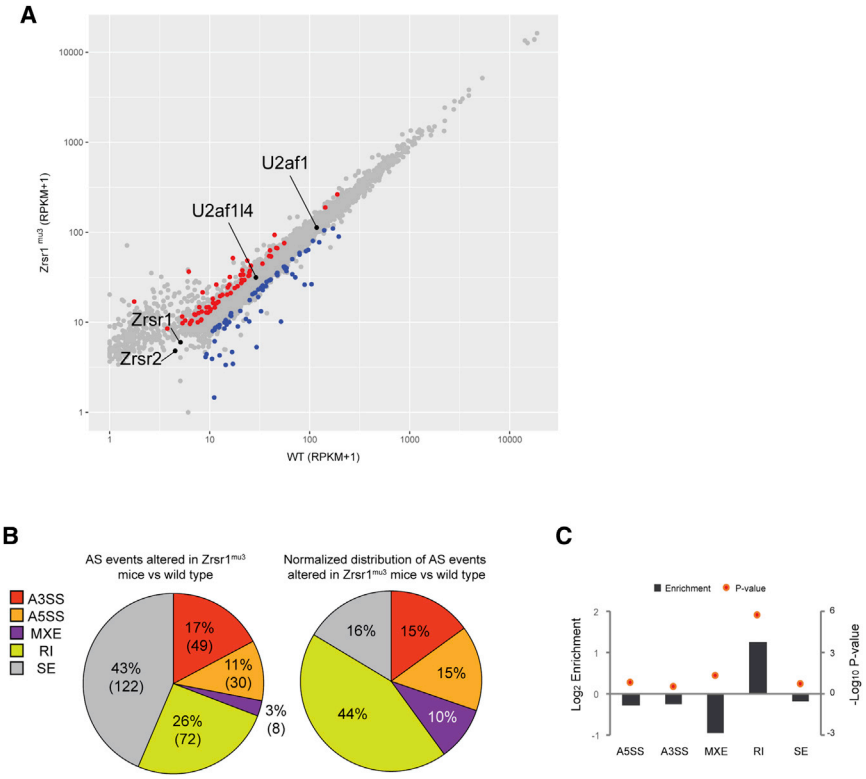

Figure 5. RNA-Seq Analysis of Gene Expression and Alternative Splicing Alterations in *Zrsr1*^{mu3} Mice Testis

(A) Scatterplot of cRPKM of *Zrsr1* ^{mu3} testes compared with controls at day 15. Blue dots represent significantly downregulated transcripts, while red dots show significantly upregulated transcripts ($p < 0.01$, fold-change of average cRPKM > 0.4). Grey dots indicate unchanged transcripts. cRPKM represents average of 4 WT and 5 *Zrsr1* ^{mu3} samples.

(B) Distribution of categories of alternative splicing (AS) events differing in *Zrsrs1*^{mu3} versus WT mouse testis, without (left) or normalized (right) to the overall distribution of the event categories in mouse transcriptomes. Numbers of each class of event are indicated in parenthesis.

(C) Log values of fold enrichment and –log of fold enrichment p values are provided for each AS category in the lower panel. CE, cassette exons; A3SS, alternative 3′ splice sites; A5SS, alternative 5′ splice sites; MXE, mutually exclusive exons; RI, retained introns.

blot analyses using anti-V5 antibodies in the context of the reconstitution experiments described above. The results revealed that both the WT and mutant protein interact with SF3B1, a core component of spliceosome required for branch point recognition at 3′ splice sites of U2 and U12-type introns, and with ZCRB1, a component of the minor spliceosome, although the interactions were somewhat reduced in the mutants, with the exception of the interaction between ZCRB1 and ZRSR1^{mu3} (Figure 4E). As expected, interactions were more apparent when the endogenous ZRSR1 and ZRSR2 proteins were knocked down.

Given our failure to generate antibodies able to detect endogenous mouse ZRSR1, we attempted to detect the presence of WT and mutant ZRSR1 in immunoprecipitates of ZCRB1 from mouse testes by targeted proteomics. Immunoprecipitation using anti-ZCRB1 antibodies followed by parallel-reaction monitoring (PRM) identified peptides corresponding to ZRSR1 both in WT and ZRSR1^{mu3} testes, demonstrating that both the WT and the truncated mutant proteins are indeed expressed (Figure S6).

U12 Intron Retention Is the Most Frequent Splicing Alteration Observed in *Zrsr1*^{mu3} Mouse Testis

To determine the molecular basis for the spermatogenesis defects observed in *Zrsr1*^{mu3} mice, we undertook RNA-seq analyses of testes from 4 WT and 5 *Zrsr1*^{mu3} animals on day 15, immediately after *Zrsr1* expression peaks in developing testis, when the majority of germ cells are at the spermatocyte stage in both WT and *Zrsr1*^{mu3} animals (Figure 2C). The expression of the other 3 paralogs in WT and *Zrsr1*^{mu3} mice was comparable (Figure 5A). We examined splicing events that were modified in *Zrsr1*^{mu3} mouse testis using MISO software (Katz et al., 2010). In total, 281 alternative splicing events were identified as modified with a minimum difference in percent spliced in (ΔPSI) of 10%. All categories of alternative splicing (AS) events were affected (Figure 5B). However, once normalized according to the overall distribution of AS events in the mouse, intron retention (IR) was the most significantly affected category (44%) (Figures 5B and 5C).

Altered splicing events were further examined using software developed by our group (https://github.com/ppapasaikas/SANJUAN/tree/master/perllib), which can be used to identify and annotate novel, non-annotated events, and quantify differences in the use of competing junctions and retained introns. We identified 234 IR events that were modified in *Zrsr1*^{mu3} testis (Table S3) displaying fold changes in intron expression |logFC (WT/mu3)| > 0.7 (Experimental Procedures). Intron retention ratio (IRR) values ranged from 0% to a maximum of 64.1%, although most of the IR events (79.5%) displayed an IRR of <10%. Likewise, the majority (86.3%) of IR events showed <10% difference in IRR (ΔIRR) between WT and *Zrsr1*^{mu3} mice (Figure S7A), although larger IRR/ΔIRR values may be difficult to detect due to efficient nuclear and cytoplasmic degradation of non-spliced RNA.

Because human ZRSR2 has been implicated in both U2 and U12 intron splicing (Shen et al., 2010), we distinguished between these two intron classes. First, we updated the U12 intron database using the mouse genome mm10 (Experimental Procedures; Table S4). This resulted in the identification of 647 U12 introns (466 GT/AG and 181AT/AC). Thirty-six percent of increased IR events observed in *Zrsr1*^{mu3} mice (84 out of 234 events) corresponded to the U12 class of introns, a very significant (>70-fold) enrichment over the overall proportion of U12

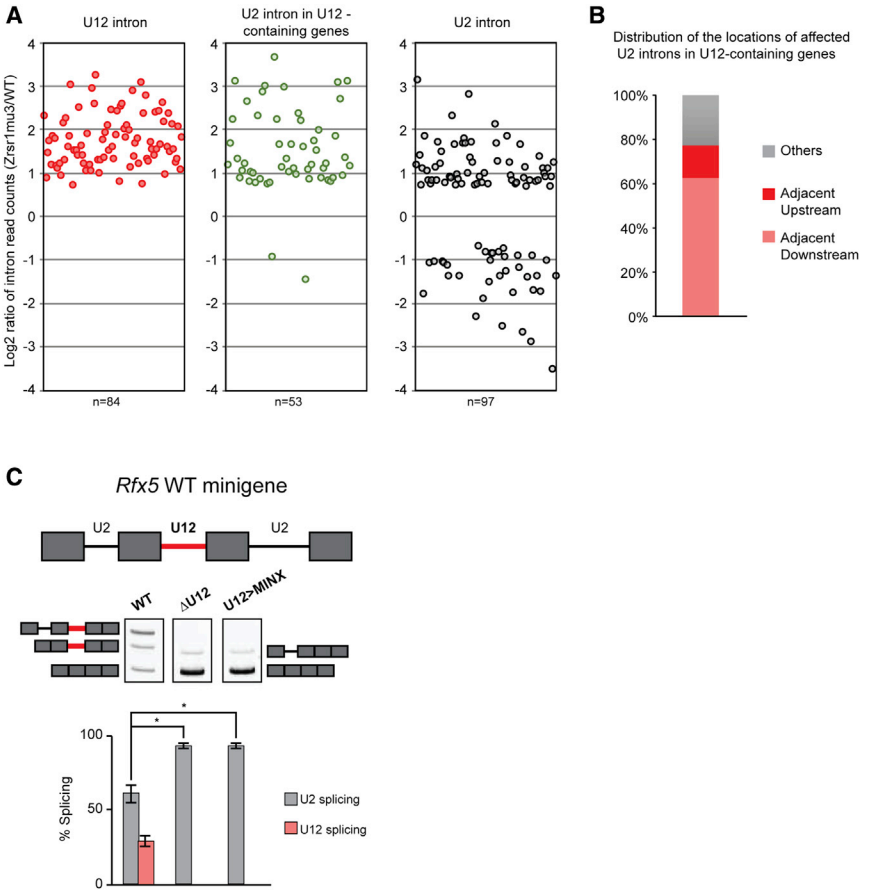

Figure 6. U12 and U2 Intron Retention in *Zrsrs1*^{mu3} Mice and Interplay between Introns Spliced by the Major and Minor Spliceosomes

(A) Number and fold changes of intron retention in *Zrsr1*^{mu3} compared to WT mouse testis (measured as log2 ratio of intron read counts in *Zrsr1*^{mu3} versus WT) for different intron categories, as indicated.

(B) Distribution of the locations of affected U2 introns in *Zrsr1*^{mu3} mice relative to U12 introns present in the same gene.

(C) Minigene splicing assays indicate that splicing of U12 intron 5 influences U2 intron 4 splicing. Top: diagram of the exon/intron structure of the genomic region included in the Rfx5 minigene. Middle: RT-PCR analysis of minigene-derived transcripts isolated from HEK293 cells transfected with the indicated constructs (WT, WT sequence; Intron 5, deletion of intron 5; Intron5 > MINX, construct in which Rfx5 intron 5 was replaced with a U2 intron from an efficiently spliced adenovirus major-late promoter transcript intron). The positions of the different spliced/partially spliced products are indicated. Bottom: quantification of the percentage of intron 4 (U2) and intron 5 (U12) splicing for five independent biological replicates. The values are the average ± SD (error bars), $p < 0.01$ versus WT minigene (t test).

introns in the mouse transcriptome (0.5%) (Figure 6A). Among the 573 genes containing U12 introns (in total 647 introns) in the mouse genome, 522 genes (corresponding to 589 U12 introns) were expressed in WT and/or *Zrsr1*^{mu3} testis (cRPKM >1). Thus, 14.3% (84 out of 589 introns) of U12 introns expressed in testis were affected in *Zrsr1*^{mu3} mice. These findings suggest a specific role in U12 intron splicing for ZRSR1 that cannot be provided in mouse testis by any of the other 3 paralogs.

Twenty-three percent (53 out of 234 events) of the IR events corresponded to U2 introns within U12-containing genes. Remarkably, 77% (41 out of 53 U2 introns) of these are located immediately upstream or (more commonly) downstream of the U12 introns, suggesting mutual influences between neighboring U12 and U2 introns (Figures 6A, middle panel, and 6B). In fact, 13 out of the 41corresponding adjacent U12 introns were also identified as more retained in *Zrsr1*^{mu3} mice. U2 IR was also observed in genes lacking U12 introns (36% of the events), although these changes in IR were generally reduced over those detected in the affected U12 introns (Figures 6A, compare left and right panels, and S7A). In contrast, the distribution of IR changes was similar between affected U12 introns and U2 introns within U12 intron-containing genes, with most events featuring a more than 2-fold increase in intron read counts in *Zrsr1*^{mu3} mice (Figure 6A, compare left and central panels). Surprisingly, 36.1% of the U2 introns affected showed less retention than in WT mice (Figures 6A, right panel, and S7A), which could reflect either a direct repressive effect of ZRSR1 or indirect effects of the mutant protein on a subset of introns. The majority (93.3%) of the genes displaying elevated IR showed no detectable changes (|Log2FC| < 0.5) in overall expression.

To validate the U12 intron splicing abnormalities observed in *Zrsr1*^{mu} mice, we analyzed U12 IR events identified with MISO by semiquantitative RT-PCR of RNAs from *Zrsr1*^{mu3}, *Zrsr1*^{mu6} and control WT adult testes. Significant increases in U12 IR were detected in both *Zrsr1*^{mu3} and *Zrsr1*^{mu6} mice compared with WT for all 7 U12 introns examined (Figure S7B). Increases in IR ranged from 2- to 30-fold, with cases in which IR corresponded to >30% of the total transcripts. Similar results were obtained by qRT-PCR (Figure S7C), although fold IR change estimates were somewhat higher using this method. IR changes were similar for *Zrsr1*^{mu3} and *Zrsr1*^{mu6} mice, suggesting that both mutant proteins are non-functional, consistent with the similar associated mice phenotypes. As predicted by MISO analysis, we observed no changes in the retention of *Gpaa1* and *Hdac10* U2 introns.

Our SANJUAN software also detected other alternative splicing differences between WT and *Zrsr1*^{mu3} mice, including 268 skipped exons, 57 alternative 3′ splice sites, and 19 alternative 5′ splice sites with a minimum ΔPSI of 15%. Among these, we observed in *Zrsr1*^{mu3} mice 15 aberrant splicing events associated with U12 introns (Table S3). On several occasions, U2 5′ or 3′ splice sites were activated within an exon or a U12 intron or

within the flanking U2 introns. These sites were spliced to (U2) 3′/5′ splice sites resulting in partial IR, truncated exons and/or exon skipping (Figure S8A). These observations further support the possibility of an interplay between major and minor spliceosomes.

Candidate genes containing affected U12 introns that could underlie the spermatogenesis defects include *Mei1*, *Catsper2*, *Htt*, *Catsper1*, *Spo11*, *Diap2*, *Inpp5B*, *Oca2*, *Spag16*, and *Taf7L*. *Spo11* and *Mei1* are required for chromosome synapsis in meiosis I and their deletion results in arrest at the zygotene stage (Baudat and Keeney, 2001; Libby et al., 2002; Smirnova et al., 2006). As shown in Figures 3 and S2, some seminiferous tubules in *Zrsr1*^{mu3} testis arrested at the spermatocytes stage, correlating with reduced Mei1 expression. Thus, increased U12 IR in *Mei1* (as well as Spo11, in which we also identified a U12 intron retention event) could contribute to the observed meiotic arrest (Figure S8C). In addition, the timing of arrest at the zygotene stage is consistent with meiotic sex chromosome inactivation (MSCI), which occurs during prophase I in the male germline. The expression of 82% of all X-linked genes including *Zrsr2* has been reported as suppressed via MSCI (Mueller et al., 2008; Namekawa et al., 2006). The loss of *Zrsr1* could be offset by *Zrsr2* expression before MSCI, and the phenotype in *Zrsr1*^{mu3} testis may conceivably emerge after MSCI, at the time when *Zrsr2* is silenced. Low sperm counts were observed in *Zrsr1*^{mu3} testis (Figure 2F) indicating that some spermatocytes successfully go through meiosis, most probably supported by the remaining levels of ZRSR2 protein after MSCI. Gene expression analysis identified only 131 genes (67 downregulated and 64 upregulated) differentially expressed in *Zrsr1*^{mu3} mouse testis compared with the WT (log2 ratio of cRPKM >0.4 and $p < 0.01$, Figure 5A; Experimental Procedures). Seventeen out of 40 genes examined (42%) were validated as differentially expressed in *Zrsr1*^{mu3} testis (Figure S8D). Interestingly, 65% of the validated downregulated genes contain U12 introns, suggesting that U12 intron retention in those genes leads the transcript to enter the nuclear and cytoplasmic degradation pathway and results in the decrease of total expression of the gene (Figure S8D). qRT-PCR of the 10 U12 intron-containing genes classified as relevant for spermatogenesis revealed reduced expression of total transcripts in all the 10 genes to 25 ~67% in *Zrsr1*^{mu3} testis at day 15, although they were filtered out from RNA-seq analysis due to the individual variation (Figure S8E). Taken together, these data suggest that the defect in spermatogenesis in *Zrsr1*^{mu3} mice could be attributed to mis-regulation of spermatogenesis-related genes containing U12 introns.

The U12 Intron Reduces the Efficiency of Splicing of the Upstream U2 Intron in an *Rfx5* Minigene

To investigate possible mutual influences between U2 and U12 intron splicing, a minigene containing U12 intron 5 flanked by U2 introns 4 and 6 of the *Rfx5* gene was transfected into HEK293 cells. RNA was then isolated 24 hr post-transfection and minigene-derived transcripts detected by RT-PCR (Figure 6C). Substantial levels of IR were observed both for intron 4 (U2, ~45%, corresponding to the upper band in lane 1 in Figure 6C) and for intron 5 (U12, ~70%, corresponding to upper + middle bands in lane 1 in Figure 6C). As no (U2) intron 4 retention was detected in the absence of (U12) intron 5 retention in our minigene assays (Figure 6C, lane 1), it could be that splicing of U12 intron 5 affects splicing of U2 intron 4. To test this hypothesis, U12 intron 5 was deleted from the minigene. The results revealed the efficient (~95%) removal of U2 intron 4 (Figure 6C, compare lanes 1 and 2), suggesting that the presence of the U12 intron blocks the removal of the upstream U2 intron. To confirm that this effect was indeed related to the presence of a U12 intron, intron 5 was replaced by an intron from transcripts derived from the adenovirus major late promoter, which is efficiently spliced by the U2 spliceosome (Figure 6C, lane 3). As in its absence, the replacement of intron 5 by an efficiently spliced U2 intron also resulted in efficient U2 intron 4 splicing in this minigene system. These data indicate that inhibition of a U12 intron exerts an inhibitory effect on splicing of the upstream intron, thus arguing for mutual functional influences between major and minor spliceosome machineries.

DISCUSSION

In this study, we report a physiological role of ZRSR1 in erythrocyte development, muscular strength, and spermatogenesis, by examining *Zrsr1* mutant mice lacking one of the two zinc finger domains and part of the RNA-recognition motif (RRM) of the protein. In addition, as possible explanations for the phenotypes observed, we identified, using transcriptome analyses, abnormalities in the expression and splicing of U12 introns as well as their adjacent U2 introns.

One of the first questions that arises from our observations is that, if ZRSR1 is expressed in many tissues, why do the phenotypic effects of the mutation appear to be restricted to spermatogenesis, erythrocyte development and muscle strength, and observed only in homozygous mice. We suggest that the mutant protein ZRSR1^{mu} exerts its effects mainly in tissues where its expression predominates over the expression of *Zrsr2* or other paralogs. Consistent with this, expression of the mutant protein was seen to exacerbate the U12 intron splicing defect only in *Zrsr* siRNA-treated cells and only in certain substrates (Figure 4). Thus, the truncated protein may exert its dominant effects through abortive interactions with substrate RNAs and/or with components of the minor spliceosome (Figure 4), which could be particularly critical for specific subsets of 3′ splice sites. Consistently, zinc finger domains in U2AF35 have been implicated in 3′ splice site selection (Ilagan et al., 2015).

The origin and coexistence of two parallel intron types and two machineries for their removal remains poorly understood, especially because U12-type introns are present at very low frequencies. Recent findings point to a role of U12-dependent splicing in development, disease, and cell division (König et al., 2007; Turunen et al., 2013), indicating essential functions of U12-type splicing. In addition, it is known that RNA mis-splicing is the underlying mechanism for several diseases (Chabot and Shkreta, 2016; Daguenet et al., 2015) including male infertility (Bao et al., 2014; O'Bryan et al., 2013). Further, somatic mutations in 3′ splice site recognition factors, including ZRSR2, have been attributed a role in myelodysplastic syndrome (MDS) (Thol et al., 2012; Yoshida et al., 2011) and have been also linked to splicing defects, including most U12-type introns

(Madan et al., 2015). Our RNA-seq analysis of *Zrsr1*^{mu3} mouse testis also revealed greater impact of the mutation on U12 intron retention compared to U2 intron retention, revealing functional similarities between *Zrsr1* and *Zrsr2*, consistent with *Zrsr1* being a retrotransposed copy of X-linked *Zrsr2*.

Our transcriptome and minigene assays revealed an interplay between neighboring U12 and U2 introns. Most retained U2 introns within U12-containing genes are located immediately upstream or downstream of the U12 introns (more commonly and with more pronounced changes in intron retention when located downstream; Figure S8B), similar to observations associated with *Zrsr2* mutations in MDS patients (Madan et al., 2015). This crosstalk is thought to involve effects on exon definition that could be mediated by SR proteins or other auxiliary factors (Hastings and Krainer, 2001; Wu and Krainer, 1996). Interestingly, ZRSR2 has been shown to play a role in early 3′ splice site recognition of U12 introns and in the second catalytic step of U2 intron splicing (Shen et al., 2010). It is possible that ZRSR1 also has a dual role in both spliceosomes and that the combined defect in ZRSR1 function is consequently most noticeable in adjacent pairs of U2/U12 introns. While U12 intron splicing is enhanced by the presence of flanking U2 introns (Wu and Krainer, 1996), our *Rfx5* minigene assay revealed that U12 intron retention actively inhibits splicing of the adjacent U2 intron. The removal of U12 introns is generally slower or less efficient than that of U2 introns, resulting in 2-fold higher retention steady-state RNA levels (Niemelä and Frilander, 2014; Patel and Steitz, 2003; Singh and Cooper, 2012). This difference could serve as a final check of the mRNA in the cytoplasm for post-transcriptionally control of the expression of a specific subset of genes (van den Hoogenhof et al., 2016).

U12-dependent splicing is required for development in humans, *D. melanogaster*, *A. thaliana*, and *D. rerio* (Markmiller et al., 2014; Turunen et al., 2013). We have observed the early expression of *Zrsr1* in preimplantation embryos in mice, pigs, and earlier, in cows (Bermejo-Alvarez et al., 2010). In these three mammalian species, there are two peaks of *Zrsr1* expression during preimplantation development, one at the time of embryonic genome activation, and the other at the blastocyst stage, suggesting its important function during early development. Interestingly, the main cell types that were affected in *Zrsr1*^{mu} mice correspond to cells for which a function for the minor spliceosome has been proposed to take place in the cytoplasm (Turunen et al., 2013). These include spermatocytes after nuclear envelope breakdown, enucleate hemostatic cells (e.g., mature erythrocytes), and cells capable of rapid response to changes in the local environment (e.g., muscle cells).

Spermatogenesis can be divided into a mitotic, a meiotic, and a haploid phase. Thus, spermatocytes undergo homologous recombination-mediated crossover and nuclear envelope breakdown, followed by two consecutive meiotic cell divisions. The seminiferous tubules of *Zrsr1*^{mu} mice were arrested at the spermatocyte stage suggesting a malfunction of Sertoli and/or germ cells. In our spermatogonia transplantation assays Sertoli cells from *Zrsr1*^{mu} mice were able to support spermatogenesis of WT spermatogonia suggesting that ZRSR1 is essential for normal germ cell function. According to Schmid et al., (2013), the splicing landscape is reprogrammed during mitotic-to-meiotic transition of the male germ cell cycle. Our results support an essential role for *Zrsr1* in this transition, when transcription of its principal paralog *Zrsr2* is repressed through X chromosome inactivation during spermatogenesis, and suggest that minor spliceosome-dependent splicing may be pivotal during meiotic nuclear envelope breakdown.

We observed that *Zrsr1* is the preferentially expressed *U2af35* paralog in mature erythrocytes. Consistently, specific upregulation of *Zrsr1* and downregulation of *U2af1* have been reported during erythroid differentiation (Grosso et al., 2008). Of note, our RNA-seq data identified the differential expression of genes related to iron homeostasis, including *Ftmt* (ferritin mitochondrial), *Ftl1* (ferritin light chain 1), *Tfrc* (transferrin receptor), and *Slc25a37* (solute carrier family 25 mitochondrial iron transporter, member 37). High intron retention levels in the *Slc25a37* gene and other (particularly RNA processing) genes have been reported during terminal erythropoiesis (Pimentel et al., 2016). Intron retention in *Slc25a37* is thought to provoke abnormal iron accumulation in MDS erythroblasts (Visconte et al., 2015). Thus, intron retention may act as a post-transcriptional regulator of iron homeostasis genes in erythrocytes.

Some measure of muscular weakness is associated with mutations in Ca^{2+} channels (Cain and Snutch, 2011) although loss of muscle strength can be caused by several factors, including a drop in releasable calcium from skeletal muscle SR calcium stores (Kabbara and Allen, 1999). Interestingly, altered splicing of the skeletal muscle genes chloride channel gene (*Clcn1*), bridging integrator (*Bin1*), ryanodine receptor 1 (*RyR1*), myotubularin-related 1 gene (*Mtmr1*), and sarcoplasmic/endoplasmic reticulum Ca^{2+} ATPase (*Serca*) 1 or 2 seem to contribute to myotonia, muscle weakness, and impaired calcium homeostasis (Singh and Cooper, 2012). We noted a significant reduction in Ca^{2+} released from the SR in *Zrsr1*^{mu} mice in response to stress (Figure S5G), suggesting abnormalities in Ca^{2+} flux across the sarcolemma underlying the muscle strength loss observed in mutant mice. Multiple members of gene families related to Ca^{2+} biology and ion channels show clear enrichment in U12-type introns (Ca^{2+}-dependent phospholipases, calpains, voltage-dependent Ca^{2+} channels, and sperm-specific Ca^{2+} channels, Na^+ channels, $Na^+/K^+/Cl^-/H^+$ channels, and Cl^- channels), suggesting a role for *Zrsr1* in regulating U12-type muscle-specific splicing events. Consistently, we observed misregulation of *Tnnt2* (troponin T type 2), whose alternative splicing results in many isoforms and regulates muscle contraction in response to alterations in intracellular calcium ion concentrations (Jin et al., 2008). Future analysis of minor splicing in muscle could provide further insight into the role of splicing defects in muscle-related diseases. Such a role is well documented for the major spliceosome (Daguenet et al., 2015; Scotti and Swanson, 2016).

EXPERIMENTAL PROCEDURES

Generation of *Zrsr1* Mutant Mice

Mouse *Zrsr1* (NM_011663.3) gene was targeted and five transgenic lines were successfully generated. Details are provided in the Supplemental Information. For this study, two lines with 4 and 5 nt deletions were used (*Zrsr1* mutant lines

3 and 6). Homozygotes were used in all experiments. *Zrsr1*$^{mu/+}$ did not differ phenotypically from *Zrsr1*$^{+/+}$ mice, and both genotypes were used as controls. Animal experiments were carried out in strict accordance with the recommendations stipulated in the guidelines of European Community Council Directive 2010/63/EU. Experiments were approved by the Committee on the Ethics of Animal Experiments of the INIA (permit number CEEA 2012/021).

Gene Expression Analysis: qRT-PCR

RNA extraction and qRT-PCR were conducted following standard protocols as detailed in the Supplemental Information.

Isolation of Spermatogenic, Sertoli Cells, and Spermatozoa

To isolate spermatogenic and Sertoli cells, mice were euthanized and the testes were subjected to slight collagenase-trypsin digestions for obtaining a cell suspension. Overnight culture of this cell suspension allowed to separate the Sertoli cells (attached to the culture plate) from the spermatogenic cells (cells in suspension). Detailed protocol can be found in the Supplemental Information. Spermatozoa were extracted from epididymis following standard procedures described in the Supplemental Information.

Muscle Histology and Morphometry

Histological sections were stained with H&E as well as with PicroSirius red solution. Further description is provided in the Supplemental Information.

Testis Histology, TUNEL Staining, and Sperm Staining

For histological examination, whole mouse testes were fixed in Bouin's fluid at 4°C overnight, washed in PBS, and then paraffin embedded and H&E-stained. To detect apoptotic cells, testes were fixed in 10% PFA (neutral buffered, Sigma-Aldrich, MI, USA) and sections (5-μm) were stained using the TUNEL *in situ* Cell Death Detection Kit (Roche, Basel, Switzerland) following the protocol provided by the manufacturer. Scoring of apoptosis frequency was performed by counting TUNEL fluorescent cells in 20 random seminiferous tubules in 6 WT and 6 mutant mice. Tubule cross-sections were scored as number of apoptotic cell per seminiferous tubule.

Immunocytochemistry for Mei1 Detection

Dewaxed and rehydrated testis sections were labeled with the primary anti Mei1 antibody (sc-515359, Santa Cruz Biotechnology, TX, USA) following a standard procedure (see the Supplemental Information for further details).

Spreading of Spermatocytes and Immunocytology

Spermatocytes were obtained from testes of adult *Zrsr1*^{mu} males by the drying-down technique as previously described (Peters et al., 1997) and labeled with anti SYCP3 (sc-74569, Santa Cruz) or anti γ-H2AX (ab-2893, Abcam) antibodies following a standard immunocytochemical protocol (see the Supplemental Information for further details).

DNA Methylation

DNA methylation was analyzed from 5 fertile and 5 sterile *Zrsr1*$^{mu/mu}$ mice by bisulfite conversion followed by PCR amplification, clonation, and sequencing. Detailed procedure is described in the Supplemental Information.

Complete Blood Counts

Mice were bled into EDTA-containing tubes and complete blood counts and cytological analysis performed on peripheral blood collected using EDTA-coated capillaries. Peripheral blood was diluted 10-fold into cold buffer (HBSS containing 20 mM EDTA) and subjected to automated analysis using a Bayer Advia120 hematology analyzer. Reticulocyte morphologies were scored by counting in blood smears stained with new methylene blue (Sigma-Aldrich, MI, USA) according to the manufacturer's protocol.

Testicular Germ Cell Preparation and Transplantation

Isolated spermatogenic cells were injected into testes of males pre-treated with busulfan for germline removal. As a reporter, the transgenic mice strain X^{EGFP} (Nakanishi et al., 2002) was used. Thus, spermatogenic cells of *Zrsr1*$^{mu/mu}$ mice were transferred to testis of will type mice and vice versa. After 45 or 60 days colonization of the receipt, testis was evaluated by fluorescent microscopy. For a detailed protocol, see the Supplemental Information.

Behavior Tests

Balance beam and wire hang test were conducted in WT or mutant mice as detailed in the Supplemental Information.

Calcium Contents of the Extensor Digitorum Longus and Tibialis Anterior

Total calcium of digitorum longus (EDL) and tibialis muscles was quantify following the procedure described elsewhere (Lamboley et al., 2015) and detailed in the Supplemental Information.

Calcium Flux across the Sarcolemma in Intact Extensor Digitorum Longus

Ca^{2+} flux in EDL muscle was assessed following the method described by Park et al., (2014) and detailed in the Supplemental Information.

ZRSR1 Expression Vectors and Stable Cell Lines

Human ZRSR1, mouse Zrsr1, Zrsr1^{mu3}, and mouse Zrsr1 truncated protein (219 aa) coding sequence tagged with a V5 sequence at the N terminus (V5-) were cloned in HEK293 cells as described in the Supplemental Information.

Sample Preparation for Parallel Reaction Monitoring Proteomics

For detection of endogenous mouse Zrsr1 protein testis lysates were conducted to co-immunoprecipitation using anit-ZCRB1 polyclonal antibody A304-697A, Bethyl Laboratories). Subsequently parallel reaction monitoring (PMR) by liquid chromatography-tandem mass spectrometry (LC-MS/MS) analysis was conducted following the protocol described in the Supplemental Information.

RNA-Seq Analysis

RNA-seq was performed from the testes of 4 WT mice and 5 knockout mice at day 15 as described in the Supplemental Information.

Updating the U12 Intron Database

Using mammalian U12 sequences from U12 db (http://genome.crg.es/cgi-bin/u12db/u12db.cgi), position weight matrices were generated for the donor, acceptor, and branch sites separately for U12-ATAC and U12-GTAG introns. These matrices were used to scan the introns of interest and classify the introns as U2 or U12 introns based on the mapping score.

RT-PCR for the Detection of U12 Intron Retention in Mouse Testis and in the Functional Reconstitution Experiments

Mouse testes of WT (n = 4), ZRSR1$^{mu/mu}$ line 3 (n = 4), and ZRSR1$^{mu/mu}$ line 6 (n = 3) were conducted for RT-PCR using a standard protocol. Further details are provided in the Supplemental Information.

Minigene Assay

The *Rfx5* minigene was constructed by subcloning a PCR product of the *Rfx5* gene containing exon 4 to 25 nt downstream of exon 7 amplified from mouse genomic DNA. See the Supplemental Information for further details.

Statistical Analysis

All data were collected from experiments run in triplicate and reported as the mean ± SEM. All statistical tests were performed using the software package SigmaStat (Systat Software, CA, USA). Significant differences were determined based on the Student's t test (two groups), one-way ANOVA, or two-way ANOVA followed by Tukey's post hoc test unless otherwise stated. Significance was set at $p < 0.05$.

DATA AND SOFTWARE AVAILABILITY

The accession number for the RNA-seq data reported in this paper is ArrayExpress: E-MTAB-4872.

SUPPLEMENTAL INFORMATION

Supplemental Information includes STAR Methods, eight figures, four tables, and one video and can be found with this article online at https://doi.org/10.1016/j.celrep.2018.03.028.

ACKNOWLEDGMENTS

We thank Maria I. Fabre (MIT, USA) for help with RNA-seq analyses. We thank the CRG/UPF Proteomics Unit, which is part of the "Plataforma de Recursos Biomoleculares y Bioinformáticos (ProteoRed)" supported by grant PT13/0001 of ISCIII and Spanish Ministry of Economy and Competitiveness. This work was funded by grants AGL2012-39652, BFU2014-55058-P, and AGL2015-66145 from the Spanish Ministry of Economy and Competitiveness and Japan Grants-in-Aid for Scientific Research 26830124 from the Ministry of Education, Culture, Sports, Science and Technology. K.H. was supported by Young Scientists Development Program, Research Center for Advanced Science and Technology at the University of Tokyo (funded by FUJIFILM Corporation). Work in J.V.'s lab was also supported by the European Research Council (ERC AdG - GA670146 - MASCP).

AUTHOR CONTRIBUTIONS

A.G.-A. and J.V. planned the project. R.F.-G., B. Pintado, and R.L.-B. produced the transgenic mice. A.P.L.-C., P.R.-I., N.F.B., and E.P. performed the experiments shown in Figures 1, 2, and 3. F.A., L.O., and F.R.d.F. performed the analysis of behavior. S.P.-C., E.P., and B. Planells performed the experiments shown in Figure S3. K.H. performed the experiments shown in Figures 4, 5, and 6. A.V. and J.A.S. performed spreading of spermatocytes and immunocytology. K.H., S.P.-C., P.P., P.J.R., J.V., and A.G.-A. analyzed the data. K.H., S.P.-C., J.V., and A.G.-A. wrote the paper. All authors reviewed and approved the final manuscript.

DECLARATION OF INTERESTS

The authors declare no competing interests.

Received: June 30, 2016
Revised: September 28, 2017
Accepted: March 8, 2018
Published: April 3, 2018

REFERENCES

Avarbock, M.R., Brinster, C.J., and Brinster, R.L. (1996). Reconstitution of spermatogenesis from frozen spermatogonial stem cells. Nat. Med. *2*, 693–696.

Bao, J., Tang, C., Li, J., Zhang, Y., Bhetwal, B.P., Zheng, H., and Yan, W. (2014). RAN-binding protein 9 is involved in alternative splicing and is critical for male germ cell development and male fertility. PLoS Genet. *10*, e1004825.

Baudat, F., and Keeney, S. (2001). Meiotic recombination: making and breaking go hand in hand. Curr. Biol. *11*, R45–R48.

Bellvé, A.R., Millette, C.F., Bhatnagar, Y.M., and O'Brien, D.A. (1977). Dissociation of the mouse testis and characterization of isolated spermatogenic cells. J. Histochem. Cytochem. *25*, 480–494.

Bermejo-Alvarez, P., Rizos, D., Rath, D., Lonergan, P., and Gutierrez-Adan, A. (2010). Sex determines the expression level of one third of the actively expressed genes in bovine blastocysts. Proc. Natl. Acad. Sci. USA *107*, 3394–3399.

Burge, C.B., Padgett, R.A., and Sharp, P.A. (1998). Evolutionary fates and origins of U12-type introns. Mol. Cell *2*, 773–785.

Cain, S.M., and Snutch, T.P. (2011). Voltage-gated calcium channels and disease. Biofactors *37*, 197–205.

Chabot, B., and Shkreta, L. (2016). Defective control of pre-messenger RNA splicing in human disease. J. Cell Biol. *212*, 13–27.

Daguenet, E., Dujardin, G., and Valcárcel, J. (2015). The pathogenicity of splicing defects: mechanistic insights into pre-mRNA processing inform novel therapeutic approaches. EMBO Rep. *16*, 1640–1655.

Grosso, A.R., Gomes, A.Q., Barbosa-Morais, N.L., Caldeira, S., Thorne, N.P., Grech, G., von Lindern, M., and Carmo-Fonseca, M. (2008). Tissue-specific splicing factor gene expression signatures. Nucleic Acids Res. *36*, 4823–4832.

Hastings, M.L., and Krainer, A.R. (2001). Functions of SR proteins in the U12-dependent AT-AC pre-mRNA splicing pathway. RNA *7*, 471–482.

Hayashizaki, Y., Shibata, H., Hirotsune, S., Sugino, H., Okazaki, Y., Sasaki, N., Hirose, K., Imoto, H., Okuizumi, H., Muramatsu, M., et al. (1994). Identification of an imprinted U2af binding protein related sequence on mouse chromosome 11 using the RLGS method. Nat. Genet. *6*, 33–40.

Ilagan, J.O., Ramakrishnan, A., Hayes, B., Murphy, M.E., Zebari, A.S., Bradley, P., and Bradley, R.K. (2015). U2AF1 mutations alter splice site recognition in hematological malignancies. Genome Res. *25*, 14–26.

Jin, J.P., Zhang, Z., and Bautista, J.A. (2008). Isoform diversity, regulation, and functional adaptation of troponin and calponin. Crit. Rev. Eukaryot. Gene Expr. *18*, 93–124.

Kabbara, A.A., and Allen, D.G. (1999). The role of calcium stores in fatigue of isolated single muscle fibres from the cane toad. J. Physiol. *519*, 169–176.

Katz, Y., Wang, E.T., Airoldi, E.M., and Burge, C.B. (2010). Analysis and design of RNA sequencing experiments for identifying isoform regulation. Nat. Methods *7*, 1009–1015.

König, H., Matter, N., Bader, R., Thiele, W., and Müller, F. (2007). Splicing segregation: the minor spliceosome acts outside the nucleus and controls cell proliferation. Cell *131*, 718–729.

Lamboley, C.R., Kake Guena, S.A., Touré, F., Hébert, C., Yaddaden, L., Nadeau, S., Bouchard, P., Wei-LaPierre, L., Lainé, J., Rousseau, E.C., et al. (2015). New method for determining total calcium content in tissue applied to skeletal muscle with and without calsequestrin. J. Gen. Physiol. *145*, 127–153.

Li, X., Cui, X.L., Wang, J.Q., Wang, Y.K., Li, Y.F., Wang, L.Y., Wan, H.F., Li, T.D., Feng, G.H., Shuai, L., et al. (2016). Generation and application of mouse-rat allodiploid embryonic stem cells. Cell *164*, 279–292.

Libby, B.J., De La Fuente, R., O'Brien, M.J., Wigglesworth, K., Cobb, J., Inselman, A., Eaker, S., Handel, M.A., Eppig, J.J., and Schimenti, J.C. (2002). The mouse meiotic mutation mei1 disrupts chromosome synapsis with sexually dimorphic consequences for meiotic progression. Dev. Biol. *242*, 174–187.

Madan, V., Kanojia, D., Li, J., Okamoto, R., Sato-Otsubo, A., Kohlmann, A., Sanada, M., Grossmann, V., Sundaresan, J., Shiraishi, Y., et al. (2015). Aberrant splicing of U12-type introns is the hallmark of ZRSR2 mutant myelodysplastic syndrome. Nat. Commun. *6*, 6042.

Markmiller, S., Cloonan, N., Lardelli, R.M., Doggett, K., Keightley, M.C., Boglev, Y., Trotter, A.J., Ng, A.Y., Wilkins, S.J., Verkade, H., et al. (2014). Minor class splicing shapes the zebrafish transcriptome during development. Proc. Natl. Acad. Sci. USA *111*, 3062–3067.

Marks, H., Kerstens, H.H., Barakat, T.S., Splinter, E., Dirks, R.A., van Mierlo, G., Joshi, O., Wang, S.Y., Babak, T., Albers, C.A., et al. (2015). Dynamics of gene silencing during X inactivation using allele-specific RNA-seq. Genome Biol. *16*, 149.

Mueller, J.L., Mahadevaiah, S.K., Park, P.J., Warburton, P.E., Page, D.C., and Turner, J.M. (2008). The mouse X chromosome is enriched for multicopy testis genes showing postmeiotic expression. Nat. Genet. *40*, 794–799.

Nabetani, A., Hatada, I., Morisaki, H., Oshimura, M., and Mukai, T. (1997). Mouse U2af1-rs1 is a neomorphic imprinted gene. Mol. Cell. Biol. *17*, 789–798.

Nakanishi, T., Kuroiwa, A., Yamada, S., Isotani, A., Yamashita, A., Tairaka, A., Hayashi, T., Takagi, T., Ikawa, M., Matsuda, Y., and Okabe, M. (2002). FISH analysis of 142 EGFP transgene integration sites into the mouse genome. Genomics *80*, 564–574.

Namekawa, S.H., Park, P.J., Zhang, L.F., Shima, J.E., McCarrey, J.R., Griswold, M.D., and Lee, J.T. (2006). Postmeiotic sex chromatin in the male germline of mice. Curr. Biol. *16*, 660–667.

Niemelä, E.H., and Frilander, M.J. (2014). Regulation of gene expression through inefficient splicing of U12-type introns. RNA Biol. *11*, 1325–1329.

Nilsen, T.W., and Graveley, B.R. (2010). Expansion of the eukaryotic proteome by alternative splicing. Nature *463*, 457–463.

O'Bryan, M.K., Clark, B.J., McLaughlin, E.A., D'Sylva, R.J., O'Donnell, L., Wilce, J.A., Sutherland, J., O'Connor, A.E., Whittle, B., Goodnow, C.C., et al. (2013). RBM5 is a male germ cell splicing factor and is required for spermatid differentiation and male fertility. PLoS Genet. *9*, e1003628.

Pan, Q., Shai, O., Lee, L.J., Frey, B.J., and Blencowe, B.J. (2008). Deep surveying of alternative splicing complexity in the human transcriptome by high-throughput sequencing. Nat. Genet. *40*, 1413–1415.

Park, K.H., Weisleder, N., Zhou, J., Gumpper, K., Zhou, X., Duann, P., Ma, J., and Lin, P.H. (2014). Assessment of calcium sparks in intact skeletal muscle fibers. J. Vis. Exp. (*84*), e50898.

Patel, A.A., and Steitz, J.A. (2003). Splicing double: insights from the second spliceosome. Nat. Rev. Mol. Cell Biol. *4*, 960–970.

Peters, A.H., Plug, A.W., van Vugt, M.J., and de Boer, P. (1997). A drying-down technique for the spreading of mammalian meiocytes from the male and female germline. Chromosome Res. *5*, 66–68.

Pimentel, H., Parra, M., Gee, S.L., Mohandas, N., Pachter, L., and Conboy, J.G. (2016). A dynamic intron retention program enriched in RNA processing genes regulates gene expression during terminal erythropoiesis. Nucleic Acids Res. *44*, 838–851.

Sato, H., Miyamoto, T., Yogev, L., Namiki, M., Koh, E., Hayashi, H., Sasaki, Y., Ishikawa, M., Lamb, D.J., Matsumoto, N., et al. (2006). Polymorphic alleles of the human MEI1 gene are associated with human azoospermia by meiotic arrest. J. Hum. Genet. *51*, 533–540.

Schmid, R., Grellscheid, S.N., Ehrmann, I., Dalgliesh, C., Danilenko, M., Paronetto, M.P., Pedrotti, S., Grellscheid, D., Dixon, R.J., Sette, C., et al. (2013). The splicing landscape is globally reprogrammed during male meiosis. Nucleic Acids Res. *41*, 10170–10184.

Scotti, M.M., and Swanson, M.S. (2016). RNA mis-splicing in disease. Nat. Rev. Genet. *17*, 19–32.

Shen, H., Zheng, X., Luecke, S., and Green, M.R. (2010). The U2AF35-related protein Urp contacts the 3′ splice site to promote U12-type intron splicing and the second step of U2-type intron splicing. Genes Dev. *24*, 2389–2394.

Singh, R.K., and Cooper, T.A. (2012). Pre-mRNA splicing in disease and therapeutics. Trends Mol. Med. *18*, 472–482.

Smirnova, N.A., Romanienko, P.J., Khil, P.P., and Camerini-Otero, R.D. (2006). Gene expression profiles of Spo11-/- mouse testes with spermatocytes arrested in meiotic prophase I. Reproduction *132*, 67–77.

Sunahara, S., Nakamura, K., Nakao, K., Gondo, Y., Nagata, Y., and Katsuki, M. (2000). The oocyte-specific methylated region of the U2afbp-rs/U2af1-rs1 gene is dispensable for its imprinted methylation. Biochem. Biophys. Res. Commun. *268*, 590–595.

Thol, F., Kade, S., Schlarmann, C., Löffeld, P., Morgan, M., Krauter, J., Wlodarski, M.W., Kölking, B., Wichmann, M., Görlich, K., et al. (2012). Frequency and prognostic impact of mutations in SRSF2, U2AF1, and ZRSR2 in patients with myelodysplastic syndromes. Blood *119*, 3578–3584.

Turunen, J.J., Niemelä, E.H., Verma, B., and Frilander, M.J. (2013). The significant other: splicing by the minor spliceosome. Wiley Interdiscip. Rev. RNA *4*, 61–76.

van den Hoogenhof, M.M., Pinto, Y.M., and Creemers, E.E. (2016). RNA Splicing: Regulation and Dysregulation in the Heart. Circ. Res. *118*, 454–468.

Visconte, V., Avishai, N., Mahfouz, R., Tabarroki, A., Cowen, J., Sharghi-Moshtaghin, R., Hitomi, M., Rogers, H.J., Hasrouni, E., Phillips, J., et al. (2015). Distinct iron architecture in SF3B1-mutant myelodysplastic syndrome patients is linked to an SLC25A37 splice variant with a retained intron. Leukemia *29*, 188–195.

Wang, E.T., Sandberg, R., Luo, S., Khrebtukova, I., Zhang, L., Mayr, C., Kingsmore, S.F., Schroth, G.P., and Burge, C.B. (2008). Alternative isoform regulation in human tissue transcriptomes. Nature *456*, 470–476.

Wu, Q., and Krainer, A.R. (1996). U1-mediated exon definition interactions between AT-AC and GT-AG introns. Science *274*, 1005–1008.

Yoshida, K., Sanada, M., Shiraishi, Y., Nowak, D., Nagata, Y., Yamamoto, R., Sato, Y., Sato-Otsubo, A., Kon, A., Nagasaki, M., et al. (2011). Frequent pathway mutations of splicing machinery in myelodysplasia. Nature *478*, 64–69.